Electric Mars: A large trans-terminator electric potential drop on closed magnetic field lines above Utopia Planitia

Glyn Collinson[1,2], David Mitchell[3], Shaosui Xu[3], Alex Glocer[1], Joseph Grebowsky[1], Takuya Hara[3], Robert Lillis[3], Jared Espley[1], Christian Mazelle[5,6], Jean-André Sauvaud[5,6], Andrei Fedorov[5,6], Mike Liemohn[4], Laila Andersson[7], Bruce Jakosky[7]

Corresponding author: Glyn Collinson, Heliophysics Science Division, NASA Goddard Space Flight Center, Greenbelt, MD, USA. (glyn.a.collinson@nasa.gov)

[1]NASA Goddard Spaceflight Center,

Abstract.

Parallel electric fields and their associated electric potential structures play a crucial role in ionospheric-magnetospheric interactions at any planet. Although there is abundant evidence that parallel electric fields play key roles

Greenbelt, Maryland, USA.

[2]Institute for Astrophysics and Computational Sciences, The Catholic University of America, Washington, District of Columbia, USA

[3]Space Sciences Laboratory, University of California, Berkeley, USA

[4]Space Physics Research Laboratory, University of Michigan, Ann Arbor, Michigan, USA

[5]CNRS, Institut de Recherche en Astrophysique et Planétologie, Toulouse, France

[6]University Paul Sabatier, Toulouse, France

[7]Laboratory For Atmospheric and Space Physics, Boulder, Colorado, USA

in Martian ionospheric outflow and auroral electron acceleration, the fields themselves are challenging to directly measure due to their relatively weak nature. Using measurements by the SWEA instrument aboard the NASA *Mars Atmosphere and Voltatile EvolutioN (MAVEN)* Mars Scout, we present the discovery and measurement of a substantial ($\Phi_{MARS} = 7.7 \pm 0.6V$) parallel electric potential drop on closed magnetic field lines spanning the terminator from day to night above the great impact basin of Utopia Planitia, a region largely free of crustal magnetic fields. A survey of the previous 26 orbits passing over a range of longitudes revealed similar signatures on 7 orbits, with a mean potential drop (Φ_{MARS}) of 10.9 $\pm$ 0.8 V, suggestive that although trans-terminator electric fields of comparable strength are not ubiquitous, they may be common, at least at these northerly latitudes.

1. Introduction

Although magnetic field aligned electric potentials play an important role in planetary ionosphere-magnetosphere interactions, very little is known about electric potential structures at Mars. However, there is abundant evidence for Martian parallel electric fields in charged particle data from the NASA *Mars Global Surveyor* (MGS), the ESA *Mars Express* (MEX), and the NASA *Mars Atmosphere and Voltatile EvolutioN (MAVEN)* Mars Scout class mission [*Jakosky et al.*, 2015]. To date, discussions of Martian parallel electric fields in the literature have focused on two processes: **A.)** ion outflow and **B.)** auroral acceleration.

Ionospheric outflow: Electric fields play a central role in several important ionospheric transport and loss processes at both Mars and Venus. Ion pickup by the penetration of the (perpendicular) motional electric field of the solar wind ($-V \times B$) produces a distinct "plume" of keV ions [see e.g. *Curry et al.*, 2015, and references therein]. Ions are also accelerated by the draping and curving of the Interplanetary Magnetic Field (IMF) around the planet ($J \times B$ forces), which generates energized ion populations readily identified through their close proximity to the current sheet [*Barabash et al.*, 2007]. However, it has long been presumed that processes resulting in parallel electric fields also play a key role in ionospheric transport and escape [*Lundin et al.*, 2006a; *Dubinin et al.*, 2011]. *Frahm et al.* [2010] used fluxes of escaping photoelectrons to make an initial estimate of the escape rates of ionospheric plasmas due to the planetary ambipolar electric field ($E \approx \nabla P_e/en_e$). Later, *Collinson et al.* [2015] used field-aligned superthermal electron measurements by the Solar Wind Electron Analyzer (SWEA) [*Mitchell et al.*, 2016] aboard *MAVEN* to place an upper limit on the total potential drop of this global "polar wind like" ambipolar electric field of $\leq 2V$. Recently, *Collinson et al.* [2016] used *Venus Express* superthermal electron observations to discover the presence of an extremely powerful ($\sim 10V$) parallel electric potential drop in the ionosphere of Venus, finding it to be stable, persistent, and capable of accelerating oxygen ions directly to escape velocities in an "electric wind". Thus Venus' planetary electric potential is important for ion escape and global, whereas at Earth it is weaker ($\leq 2V$ *Coates et al.* [1985]) and confined to the magnetic poles. Given the lower Martian gravity, a $\geq 2V$ electric potential drop would be similarly effective in accelerating Oxygen ions to escape velocity. Thus, whilst parallel electric potentials are thought to play a key role in ion outflow, the direct evidence for their existence at Mars is currently ambiguous.

Auroral acceleration: The evidence for the presence of Martian parallel potential drops is less ambiguous with regards to auroral electron acceleration above the Martian crustal anomalies. *Lundin et al.* [2006b] reported the discovery by MEX of locally accelerated electrons and ions on the deep nightside of Mars, with ion fluxes sufficient to produce a bright discrete aurora. *Brain et al.* [2006] presented collected MGS and MEX observations of peaked electron energy spectra at the crustal anomalies similar to terrestrial auroral electrons, finding that the most energetic examples occurred during the passage of space weather storm events, similar to the onset of sub-storms at Earth. *Lundin et al.* [2006c] further examined Martian auroral plasma acceleration, finding monoenergetic counterstreaming accelerated ions and electrons consistent with field-aligned electric currents and electric field acceleration. A further study by *Halekas et al.* [2008] of Martian auroral electrons observed by MGS found clear evidence for field-aligned currents, and discrete electron acceleration events reminiscent of the terrestrial auroral zone. *Dubinin et al.* [2008] reported observations of electron inverted "V" structures by both MGS and MEX, similar to events in Earth's auroral acceleration regions, raising the hypothesis that localized aurora on Mars are also generated by electron acceleration through parallel electric fields. A follow up study by [*Dubinin et al.*, 2009] reported the observation of auroral activity on numerous orbits of MEX during a two week period, implying that the auroral acceleration, and therefore the accelerating parallel electric potential drops, are a stable phenomenon, albeit spatially localized.

In this study we present field-aligned electron measurements by *MAVEN* SWEA to report the new discovery of large ($\sim 10V$) electric potential drops along closed magnetic field lines which span the terminator of Mars, connecting the dayside and nightside ionospheres. Although the detection of a trans-terminator electric potential is novel, it is important to note that the existence of closed trans-terminator magnetic field lines at Mars is well established in the literature. For example, in their survey of electron data from Mars Express (MEX), *Frahm et al.* [2006] noted that photoelectrons were occasionally seen beyond the sunlit ionosphere, suggesting magnetic connectivity between dayside and nightside ionosphere, although without a magnetometer to organize electron spectra by pitch angle it was not possible to confirm this. *Liemohn et al.* [2006] predicted such connectivity with magnetohydrodynamic (MHD) model results, tracing thousands of field lines in a search for day-night connectivity. Furthermore, *Liemohn et al.* [2007] explicitly looked for this trans-terminator magnetic connection in their analysis of MHD simulations for the initial auroral observation conditions, concluding that field lines can connect from many locations across the dayside to the nightside ionosphere.

2. Method

In this section, we describe how electric potential drops may be directly measured through examination of outflowing and inflowing planetary electrons, using a technique successfully employed at Earth to measure the large (~$20V$) parallel potential drops that occur above orbiting spacecraft (i.e. between ~$3800km$ and the magnetopause) [*Winningham and Gurgiolo*, 1982; *Wilson et al.*, 1997; *Kitamura et al.*, 2012].

2.1. Measurement topology

First let us consider a simplified example. Figure 2 shows a sketch of the overall measurement topology. *MAVEN* is above the Martian terminator, on a "closed" magnetic field line (black) which we define as having both ends of the field line intersecting the electron exobase at a "footpoint". In Mars' complex magnetic environment, such a closed topology might result from a fringe field of a crustal magnetic remanent, or from a draped Interplanetary Magnetic Field line that passes below the exobase at both footpoints. For the purposes of this study, we do not differentiate and use the nomenclature "closed" for either case: all that matters is that the ionosphere is magnetically disconnected from the solar wind, and the spacecraft connected to the ionosphere on both ends of the magnetic field line on which it is located. Since electrons (unlike ions) move effectively instantaneously along field lines and are excellent tracers of magnetic connectivity, such a closed field topology can be established by the presence of ionospheric photoelectrons and the absence of inflowing solar wind electrons which otherwise readily have access to the topside ionosphere [*Brain et al.*, 2007]. In this study, we consider a closed "trans-terminator" field line, with one footpoint on the dayside ionosphere, and the other footpoint terminating below the exobase in the nightside ionosphere.

The existence of such closed trans-terminator magnetic field lines at Mars is well established in the literature. For example, in their survey of electron data from Mars Express (MEX), *Frahm et al.* [2006] noted that photoelectrons were occasionally seen beyond the sunlit ionosphere, suggesting magnetic connectivity between dayside and nightside ionosphere, although although without a magnetometer to organize electron spectra by pitch angle it was not possible to confirm this. *Liemohn et al.* [2006] predicted such connectivity with magnetohydrodynamic (MHD) model results, tracing thousands of field lines in a search for day-night connectivity. Furthermore, *Liemohn et al.* [2007] explicitly looked for this trans-terminator magnetic connection in their analysis of MHD simulations for the initial a[illegible] observation conditions, concluding that field lines can connect from many locations across the dayside to the nightside ionosphere.

In this example, there is a $20V$ electric potential drop distant from the *MAVEN*, occurring somewhere between the spacecraft and the nightside ionosphere. In this schematic, two electrons are created in the dayside ionosphere: electron №1 with an energy of $30eV$, and electron №2 with an energy of $20eV$. Both pass *MAVEN* on their way to the nightside, and both are retarded equally by the electric force. Electron №1 is slowed to an energy of 10eV and impacts the nightside atmosphere. However, electron №2 is at just a low enough energy that it is stopped and then reflected back towards the dayside. This electrostatic mirror conserves energy, so any reflected electrons that are observed by $MAVEN$ will have regained their original energy. If large numbers of such electrons were created in the dayside ionosphere, $MAVEN$ will observe an equal flux of the lower energy ($20eV$) electrons coming from both the dayside source, and the nightside electrostatic mirror. However, although the lower energy ($20eV$) electrons will be virtually isotropic (by which we mean equal fluxes flowing from the dayside and nightside), the higher energy ($30eV$) electrons will be strongly anisotropic (by which we mean higher fluxes flowing from the dayside than from the nightside).

Whilst such a potential structure reflects negatively charged electrons back up to the spacecraft, it is important to note that positively charged ions would be accelerated away from the spacecraft, into the nightside. For comparison with electrons, Figure 2C shows how an ion (I^+) would be affected by such a potential drop. The hypothetical ion passes $MAVEN$ at 20 eV, is accelerated to 40 eV, and lost in the nightside ionosphere. Thus, under this topology, $MAVEN$ is remote from the ion acceleration region, and thus will not observe any change in ion energies since this process is happening at a distance from the spacecraft. Additionally, whilst superthermal electrons effectively move instantaneously along such a relatively short magnetic field line, ions move considerably slower due to their substantially greater mass. Electrons are therefore the best particles to use to probe field-aligned electric potential structures.

2.2. Simulated example SWEA electron spectra

Having established the basic overall topology we shall now move from hypothetical test particles to simulations of realistic Martian electron energy spectra. We shall first consider the control case where no parallel electric fields are present, and then examine how the energy spectra of Martian ionospheric electrons are affected by the presence of our hypothetical $20V$ electric potential drop.

Description of Mars-STET model: The simulated spectra in this study were generated using the Mars SuperThermal Electron Transport (STET) model [*Liemohn et al.*, 2003; *Xu and Liemohn*, 2015; *Xu et al.*, 2015], based on the earlier Earth version of the STET code [*Khazanov and Liemohn*, 1995]. STET is a time-dependent, multi-stream model that solves the gyro-averaged Boltzman equation to self-consistently calculate the flux of superthermal electrons at any point along a single magnetic flux tube. STET self-consistently models the generation of photoelectrons from a simulated Martian atmosphere from a given solar irradiance, and then simulates their transport to the nightside along the field line above the superthemal electron exobase [e.g. *Xu*, 2015; *Xu et al.*, 2016]. STET includes electron-neutral inelastic and elastic collisions, as well as Coulomb collisions with thermal electrons and ions.

For this particular simulation, the magnetic field line is assumed to be symmetric about the terminator, with a maximum field strength of 20nT at the two footpoints (one in the dayside, one on the nightside), and a minimum field strength of $10nT$ at the 400km altitude above the terminator. The dayside footprint (the location where the field line intersects the electron exobase) of the field line is set at 85° solar zenith angle (SZA) and the other in darkness (i.e. no photoionization production). The models of both the neutral atmosphere and thermal plasma environment along the field line are obtained from the Mars Global Ionosphere and Thermosphere Model (M-GITM) [*Bougher et al.*, 2015]. Solar irradiance is obtained using the Hinteregger-81 model [*Hinteregger et al.*, 1981], with an Earth F10.7 of 130 solar flux units.

Figures 2A,B show simulated field-aligned and anti-aligned electron spectra for two different strengths of electric potential drop: 2A.) an electric potential so weak that it cannot be measured, and 2B.) a hypothetical 20V potential drop, comparable to the large-scale potential drops observed at high altitudes at Earth.

Case A.) - No measurable electric potential: Let us assume *MAVEN* is situated above the terminator of Mars, and is on a closed magnetic field line that has one footpoint in the dayside atmosphere, and the other footpoint somewhere on the nightside (as in Figure 2C). Consistent with the MAVEN observations to be presented later, electrons outflowing from the dayside ionospheric source region are shown in red, and the returning electrons, inflowing back from the nightside are shown in blue. Ionospheric photoelectrons exhibit three key features: **1.)** a cluster of sharp peaks (unresolved) from 23 to 27 eV resulting from the photoionization of CO_2 and O by the intense 30.4-nm He-II line in the solar EUV spectrum; **2.)** an abrupt cut-off at ≈75eV due to a sharp drop in the intensity of the solar irradiance at wavelengths shorter than 16nm [*Gan et al.*, 1990; *Richards and Peterson*, 2008], referred to as the “Aluminium (Al) Edge"; and **3.)** a peak of oxygen auger electrons at $\sim 500eV$ due to K-shell ionization of CO2 and O by soft X-rays.

In the absence of any appreciable electric potential drop (Figure 2A), the only electrons returning from the nightside are those which have been magnetically reflected or backscattered from the nightside footpoint (blue spectrum). Although there are sources of electrons on the nightside *Fowler et al.* [2015], these are much weaker than dayside photoproduction, and thus any trans-terminator magnetic field will exhibit a strong pitch angle anisotropy in superthermal electrons at all energies [*Brain et al.*, 2007].

Case B.) - A hypothetical +20V electric potential drop: Now let us impose a hypothetical $+20V$ electric potential drop along the closed magnetic field line, occurring somewhere between the location of *MAVEN* and the nightside footpoint, as in Figure 2C. Figure 2B shows a sketch of how this hypothetical $+20V$ electrostatic mirror will effect the energy spectra of photoelectrons observed by *MAVEN*. Electrons are now isotropic below $20eV$ (by which we mean a quasi-uniform flux at all pitch angles), with all electrons below this energy being reflected back to the spacecraft. However, above this energy, electron distributions transition from isotropic to anisotropic, with greater fluxes coming from the dayside, as electrons above this transition energy have sufficient velocity to overcome the electric potential and impact the nightside atmosphere, and the only electrons returning are those which have been magnetically reflected or backscattered.

Thus, the total magnitude of electric potential drop may be directly measured through examination of at what energy the outflowing and inflowing electrons transition from isotropy to anisotropy. This transition is very sharp [*Kitamura et al.*, 2012], occurring in less than the energy channel bin width of our instrument and therefore the magnitude of the electric potential drop can be unambiguously determined from the energy at which the ratio between outflowing and inflowing electrons diverges from unity.

It is also important to note that this (isotropic to anisotropic) "transition" feature is specific to electrostatic mirrors. Whilst a magnetic mirror might also reflect particles back to the dayside, magnetic mirrors also produce loss cones, and are energy independent and adiabatic. Therefore, magnetic mirroring will not create this specific type of energy-dependent transition from isotropic to anisotropic distributions, and thus we may unambiguously infer the presence of an electrostatic mirror from the presence of such a feature.

Description of MAVEN-SWEA: The MAVEN Solar Wind Electron Analyzer is a top-hat electrostatic plasma analyzer mounted on the end of a 1.5m boom, and is equipped with electrostatic deflector plates which give it a view of 80% of the sky. It measures electrons over the energy range of 3-4600eV with a resolution of 17% ($\Delta E/E$). SWEA operates in two data collection modes: "ionospheric mode" (when MAVEN is below 2000km), and "solar wind" mode (>2000km). Each mode creates two data streams; a "burst mode" and a lower resolution "survey mode" (see table 4 of *Mitchell et al.* [2016] for a summary of SWEA operational modes). Due to the limited data rates available to planetary spacecraft such as MAVEN, only a fraction of burst mode data can be telemetered back. The event presented later in this paper represents our best current example, partly because ionospheric burst mode data was available, providing 64 energy bins and 8-sec cadence for energy/angle (3D) distributions, and 64 energy bins and 2-sec cadence for pitch angle distributions (PADs). For full details of SWEA, see *Mitchell et al.* [2016].

3. Evidence for a trans-terminator electric potential at Mars

In this section we present our current best example of a signature consistent with a trans-terminator electric field, occurring on the 3rd of March 2015. Figure 3 shows a map of the relavent orbit geometry (№ 821), and Figure 4 shows *MAVEN* observations for the low-altitude portion of orbit № 821. Periapsis was in the northern hemisphere near the terminator. The light blue line running parallel to the orbital path in Figure 3 shows the region from which *MAVEN* data are shown in Figure 4. Altitude (4A), and three-component magnetometer measurements (4B) are shown for reference and context. Figure 4C shows omni-directional energy spectra measured by SWEA, with time on the x-axis (with the same range as 4A,B), energy in eV on the y-axis, and colour denoting the $\log_{10}$ of differential energy flux in $eV cm^{-2} sr^{-1} s^{-1} eV^{-1}$.

Shown beneath are three SWEA electron scans which have been ordered by the magnetic field vector. In all three scans, the only electron populations visible are planetary photoelectrons. Since we observe no evidence for any inflowing solar wind electrons [see e.g. *Collinson et al.*, 2015], we determine that all three scans were taken when *MAVEN* was on closed magnetic field lines. Each scan (α, β, γ) shows two spectra: one a field-aligned spectrum (averaged within $\pm 60°$ of $\hat{\mathbf{B}}$) and the other an anti-aligned **spectrum** (averaged within $\pm 60°$ of $-\hat{\mathbf{B}}$). The two spectra have been coloured so that, consistent with Figure 2, red denotes the distribution of tailward flowing electrons, and blue the sunwards flowing distribution. Below each spectra is a plot showing the ratio of outflowing to inflowing electron fluxes. Full 3D pitch angle distributions for each scan are also shown in Figure 5.

Scan alpha: (“α" - left panel) represents the case where both footpoints of the closed magnetic field line passing through *MAVEN* are in the dayside photoproduction region, and thus the energy spectra of electrons traveling parallel and anti-parallel to the field are the same.

Scan beta: (“β" - center panel) shows the case similar to the simulated electrons in Figure 2A where *MAVEN* is now on a closed magnetic field line that spans the terminator, but there is no evidence for electrostatic mirroring. Consistent with our simulation, the only electrons inflowing from the nightside (blue) are magnetically reflected or backscattered, with a diminished flux compared to those outflowing from the source region (red).

Scan gamma: (“γ" - right panel), was measured just over 45 minutes later, when *MAVEN* was at 106° Solar Zenith Angle (SZA), above the Utopia Planitia impact basin, where there are no measurable crustal magnetic sources. *MAVEN* was still on closed magnetic field lines, and would be until ∼11:46, at which point connection to the solar wind is evident in the increase in flux at all energies in the SWEA spectrogram (Figure 4C). The outflowing (red) spectra are similar to the outflowing photoelectron spectra in scans α, β, albeit at a lower flux as the source region from which these electrons are outflowing from appears to be closer to the terminator with a lower photo-production rate. Above $6.5eV$ the electron distributions are anisotropic, consistent with our simulations of backscattered photoelectrons on closed trans-terminator magnetic field lines. However unlike scan β, below $6.5eV$ the electron pitch-angle distribution transitions to isotropic, with equal fluxes of inflowing (blue) and outflowing (red) electrons. This behaviour can be explained by an electrostatic mirror (Figure 2B), and is consistent with similar (isotropic to anisotropic) transitions presented at Earth by *Kitamura et al.* [2012] associated with the presence of large parallel electric potential structures at high altitudes.

Correcting for the electrostatic spacecraft potential: As electrons arrive at *MAVEN* they fall through an additional electric potential drop due to the electrostatic charging of the spacecraft. If the spacecraft is negatively charged, all electrons are slowed, whereas if the spacecraft is positively charged all electrons are accelerated towards the detector, resulting in an energy shift in the spectra of both inflowing and outflowing electrons. Therefore, the 6.5 eV transition from isotropic to anisotropic pitch angle measured in scan γ corresponds to the total potential drop (Φ_{TOTAL}) of +6.5 V, with a $\pm$0.5 V uncertainty arising from the width of the energy bin at which the transition occurred. However, Φ_{TOTAL} is the sum of the Martian potential drop (Φ_{Mars}) and the spacecraft potential (Φ_{SC}). Using the *MAVEN* Langmuir Probe and Waves (LPW) experiment, we may independently measure the spacecraft potential during scan γ, finding $\Phi_{SC} = -1.5 \pm 0.5$ V. Thus, we may correct for the spacecraft potential to determine the magnitude of the Martian electric potential drop (Φ_{Mars}) using equation 1.

$$\Phi_{Mars} = \Phi_{Total} - \Phi_{SC} \tag{1}$$

Applying this correction, we find that the Martian component of the total field-aligned electric potential drop was $\Phi_{Mars} = 7.7 \pm 0.7V$.

Expected lack of effect on local ions: As shown in Figure 1, although such a distant electric potential structure reflects electrons below the "transition" energy (in the case of scan γ, 6.5 eV) from the nightside back to the spacecraft, we would not expect to see any change in the behavior of the local ion population. This is because while the distant $\approx -8V$ electric potential is reflecting negatively charged ($< 8\ eV$) electrons back up towards *MAVEN*, it is accelerating positively charged ions away from the spacecraft and down into the distant nightside ionosphere. Therefore, while the potential structure must be accelerating ions, this acceleration is occurring at some distance from the spacecraft, and since *MAVEN* is effectively "upstream" of this process we would not expect to see any effect on the local ion population.

Consistent with this interpretation, no obvious change in the energy of the ions was observed by MAVEN STATIC. This gives further weight to the interpretation of a distant (rather than local) electric potential structure, and full details of STATIC observations can be found in the supplemental information section S1, together with continuous SWEA pitch angle distributions, and a comparison between observed magnetic fields and crustal field models.

4. Discussion

4.1. Investigating alternative explanations

Before pursuing any further analysis, a series of simulations was first carried out to see whether the parallel and anti-parallel spectra in scan γ could be explained in some way other than an electrostatic mirror. We used the Mars-STET model to investigate the effect of magnetic field configuration, neutral densities, and thermal plasma density on the parallel and anti-parallel electron distributions.

First, asymmetric field lines are tested, with a high magnetic field strength at the footpoint in sunlight and low field strength at the footpoint in shadow (and vice versa). However, it was found that the results did not affect the electron distributions appreciably. Then, we increased the neutral density in the nightside atmosphere (to increase the collisional interaction with the neutrals) by artificially multiplying the density by factors of 5 and 10. Although this raised the superthermal electron exobase to higher altitudes, it did not affect returning photoelectron fluxes at 310 km (observational altitude). Finally, to investigate whether the equal fluxes of returning superthermal electrons below $7eV$ could be explained through coloumb scattering, the nightside ionosphere was significantly enhanced by multiplying its densities by an unrealistic factor of 100 times. We found that although at lower altitudes more uniform fluxes could be observed, at 310km, where scan γ was taken, the simulated return flux was still half of that of the outgoing flux from the source region. However, this is hardly surprising since there is no known mechanism in which backscatter can act like an electrostatic mirror, returning 100% of the incident flux only for a specific energy range.

We conclude that even large changes in the neutral and plasma densities and variations of the field magnitude at the footpoints cannot account for the observed parallel and anti-parallel energy spectra. Thus, the most plausible explanation for scan γ is electrostatic reflection resulting from a potential drop between the spacecraft and the magnetic footpoint at the nightside exobase.

4.2. A preliminary search for more events

A brief survey was undertaken to see whether any other spectral discontinuities could be observed (and the experiment repeated), or whether the trans-terminator field implied by scan γ on Orbit № 821 represented a rare or potentially unique event. To address this question we examined the 26 orbits preceding 821, finding a total of 10 electric field signatures similar to those in scan γ on 7 of the orbits, suggesting that at least at these northern latitudes, trans-terminator electric fields on closed field lines are a common occurrence. Table 1 shows a summary of each of these events, showing the orbit number, date and time, the altitude and solar zenith angle of *MAVEN* at the time of the SWEA observation, and the total potential drop (Φ_{TOTAL}) implied from the energy bin of the transition from isotropic to anisotropic pitch angle distributions, the spacecraft potential (Φ_{SC}) as measured by MAVEN-LPW, and the corrected strength of the total Martian electric potential drop (Φ_{MARS}). The uncertainty is taken from the energy resolution ($\Delta E/E = 17\%$) of SWEA and the $\approx \pm 0.5$ V uncertainty in the measurement of the spacecraft potential by LPW. Whilst Orbit № 821 represents our weakest example of a field ($\Phi_{MARS} = 7.7 \pm 0.7$ V), it remains our best because the full "burst" resolution data was available, whereas on all other orbits only the "survey" mode data was transmitted to Earth, with reduced energy sampling, reducing our ability to resolve the energy of the transition, and thus the strength of the potential drop.

Although this handful of observations does not represent a statistically significant sample, we may surmise a few properties of these Martian trans-terminator electric fields along closed magnetic fields. Firstly, with a mean strength of $\overline{\Phi}_{MARS}$ =11 V, these fields are strong enough to accelerate ionospheric O^+ and O_2^+ to escape energy, and could thus drive trans-terminator transport. Secondly, the fact that such electric fields are not observed on every trans-terminator closed field (e.g. Fig. 4 scan β) indicates that the conditions responsible for these fields are not always present.

4.3. Speculation as to their origin

An electric field in the collisionless region above the ionosphere would be expected to arise from the electron pressure gradient:

$$E_{||} \approx -\frac{\nabla P_e}{e n_e} \tag{2}$$

This mechanism is key to the formation of Earth's polar wind [*Banks and Holzer*, 1968]. At Mars, while there is unquestionably a gradient in electron pressure across the terminator, it is insufficient to explain the 11V trans-terminator potential drops reported here. Furthermore, if such large potential drops were simply the result of the pressure gradient across the terminator, then one might expect to observe such potential drops on every closed trans-terminator field line. However, this is not the case (see scan β, figure 4).

Although it is possible that such a strong ambipolar field might briefly form in response to some hypothetical dramatic transient change in the Martian ionosphere, one would not expect such a formation mechanism to create stable potential structures for whole minutes at a time, as was the case for scan γ. Thus, whilst electron pressure gradient driven electric fields must be present, they cannot satisfactorily explain these strong trans-terminator potential drops, and additional unknown physical processes must be at work.

At present, the cause of these trans-terminator electric fields on closed field lines is unknown, and we cannot propose any particular mechanism, even speculatively. This said however, any future mechanism must explain two observed features: *(1.)* the electric potential drops generated by these fields are much stronger than that of the background planetary electric field ($< 2V$ [*Collinson et al.*, 2015]), and *(2.)* the fields are sometimes but not always observed, even when the magnetic topology appears to be the same. This strongly motivates future statistical studies of parallel electric fields at Mars to see if; **a.)** if they are localized around the crustal magnetic field remanents [*Acuña et al.*, 1998; *Connerney et al.*, 1999]; **b.)** if they occur at any given longitude, latitude, and altitude; and **c.)** if they are associated with any particular upstream drivers.

5. Conclusions

At 11:46:25 on the 3rd of March 2015, the NASA *MAVEN* Mars Scout was flying above Utopia Planatia, a 3300km wide impact basin, with no measurable crustal magnetic sources. The spacecraft was ascending through 323km in altitude having just crossed over the terminator from day into night. From electron spectra measured by the Solar Wind Electron Analyzer (SWEA), we know that *MAVEN* was on a closed magnetic field line, with one magnetic footpoint on the dayside and the other on the nightside. This magnetic topology is not unusual, and indeed a similar day-to-night magnetic connection had occurred only 45 minutes previously. However, the parallel and anti-parallel electron distributions show a clear signature for electrostatic reflection, revealing the presence of a $\Phi_{MARS} = 7.7$ V potential drop from the spacecraft to the nightside footpoint of the magnetic field line. A brief survey of the previous 26 orbits revealed a total of 10 such similar signatures on 7 orbits, with a mean total electric potential drop of $\Phi_{MARS} = 10.9 \pm 0.8V$. From this small unstatistical sample, we see that such cross-terminator potentials are sometimes but not always observed, even when the conditions and magnetic topology appear to be similar, at least at these northerly latitudes.

The fact that such potential drops are not observed on every trans-terminator magnetic field line is highly suggestive that they are the result of either a localized or transient phenomena. Although the generation mechanism of these large parallel electric potential drops is presently unknown, we speculate that they may be associated with the magnetic configuration around localized crustal magnetic sources, although this is pure conjecture. Understanding their locality, origin, and their effects on the ionosphere and thermosphere of Mars are therefore prime objectives for future theory, modeling, and observational investigations.

Acknowledgments. *MAVEN* data is available from the NASA Planetary Data System. This work was partially supported by the CNES for the part based on observations with the SWEA instrument embarked on *MAVEN*.

References

Acuña, M. H., et al. (1998), Magnetic Field and Plasma Observations at Mars: Initial Results of the Mars Global Surveyor Mission, *Science*, *279*, 1676, doi: 10.1126/science.279.5357.1676.

Banks, P. M., and T. E. Holzer (1968), The polar wind, *J. Geophys. Res.*, *73*, 6846–6854, doi:10.1029/JA073i021p06846.

Barabash, S., et al. (2007), The loss of ions from Venus through the plasma wake, *Nature*, *450*, 650–653.

Bougher, S., A. Brecht, R. Schulte, J. Fischer, C. Parkinson, A. Mahieux, V. Wilquet, and A. Vandaele (2015), Upper atmosphere temperature structure at the venusian terminators: A comparison of {SOIR} and {VTGCM} results, *Planet. Space. Sci.*, (0), –, doi:http://dx.doi.org/10.1016/j.pss.2015.01.012.

Brain, D. A., et al. (2006), On the origin of aurorae on Mars, *Geophys. Res. Lett.*, *33*, L01201, doi:10.1029/2005GL024782.

Brain, D. A., R. J. Lillis, D. L. Mitchell, J. S. Halekas, and R. P. Lin (2007), Electron pitch angle distributions as indicators of magnetic field topology near Mars, *Journal of Geophysical Research (Space Physics)*, *112*, A09201, doi:10.1029/2007JA012435.

Coates, A. J., A. D. Johnstone, J. J. Sojka, and G. L. Wrenn (1985), Ionospheric photoelectrons observed in the magnetosphere at distances up to 7 earth radii, *Planet. Space. Sci.*, *33*, 1267–1275, doi:10.1016/0032-0633(85)90005-4.

Collinson, G., et al. (2015), Electric Mars: The first direct measurement of an upper limit for the Martian "polar wind" electric potential, *Geophys. Res. Lett.*, *42*, 9128–9134, doi:10.1002/2015GL065084.

Collinson, G. A., et al. (2016), The electric wind of Venus: A global and persistent “polar wind"-like ambipolar electric field sufficient for the direct escape of heavy ionospheric ions, *Geophys. Res. Lett.*, doi:10.1002/2016GL068327.

Connerney, J. E. P., et al. (1999), Magnetic Lineations in the Ancient Crust of Mars, *Science*, *284*, 794, doi:10.1126/science.284.5415.794.

Curry, S. M., J. Luhmann, Y. Ma, M. Liemohn, C. Dong, and T. Hara (2015), Comparative pick-up ion distributions at Mars and Venus: Consequences for atmospheric deposition and escape, *Planet. Space. Sci.*, *115*, 35–47, doi:10.1016/j.pss.2015.03.026.

Dubinin, E., G. Chanteur, M. Fraenz, and J. Woch (2008), Field-aligned currents and parallel electric field potential drops at Mars. Scaling from the Earths aurora, *Planet. Space. Sci.*, *56*, 868–872, doi:10.1016/j.pss.2007.01.019.

Dubinin, E., M. Fraenz, J. Woch, F. Duru, D. Gurnett, R. Modolo, S. Barabash, and R. Lundin (2009), Ionospheric storms on Mars: Impact of the corotating interaction region, *Geophys. Res. Lett.*, *36*, L01105, doi:10.1029/2008GL036559.

Dubinin, E., M. Fraenz, A. Fedorov, R. Lundin, N. Edberg, F. Duru, and O. Vaisberg (2011), Ion Energization and Escape on Mars and Venus, *Space Sci. Rev.*, *162*, 173–211, doi:10.1007/s11214-011-9831-7.

Fowler, C. M., et al. (2015), The first in situ electron temperature and density measurements of the Martian nightside ionosphere, *Geophys. Res. Lett.*, *42*, 8854–8861.

Frahm, R. A., et al. (2006), Carbon dioxide photoelectron energy peaks at Mars, *"Icarus"*, *182*, 371–382, doi:10.1016/j.icarus.2006.01.014.

Frahm, R. A., et al. (2010), Estimation of the escape of photoelectrons from Mars in 2004 liberated by the ionization of carbon dioxide and atomic oxygen, *Icarus*, *206*, 50–63, doi:10.1016/j.icarus.2009.03.024.

Gan, L., T. E. Cravens, and M. Horanyi (1990), Electrons in the ionopause boundary layer of Venus, *Journal of Geophysical Research (Space Physics)*, *95*, 19,023–19,035, doi:10.1029/JA095iA11p19023.

Halekas, J. S., D. A. Brain, R. P. Lin, J. G. Luhmann, and D. L. Mitchell (2008), Distribution and variability of accelerated electrons at Mars, *Advances in Space Research*, *41*, 1347–1352, doi:10.1016/j.asr.2007.01.034.

Hinteregger, H. E., K. Fukui, and B. R. Gilson (1981), Observational, reference and model data on solar EUV, from measurements on AE-E, *Geophys. Res. Lett.*, *8*, 1147–1150, doi:10.1029/GL008i011p01147.

Jakosky, B., et al. (2015), The mars atmosphere and volatile evolution (maven) mission, *Space Science Reviews*, pp. 1–46, doi:10.1007/s11214-015-0139-x.

Khazanov, G. V., and M. W. Liemohn (1995), Nonsteady state ionosphere-plasmasphere coupling of superthermal electrons, *J. Geophys. Res.*, *100*, 9669–9682, doi:10.1029/95JA00526.

Kitamura, N., K. Seki, Y. Nishimura, N. Terada, T. Ono, T. Hori, and R. J. Strangeway (2012), Photoelectron flows in the polar wind during geomagnetically quiet periods, *Journal of Geophysical Research (Space Physics)*, *117*, A07214, doi: 10.1029/2011JA017459.

Liemohn, M. W., D. L. Mitchell, A. F. Nagy, J. L. Fox, T. W. Reimer, and Y. Ma (2003), Comparisons of electron fluxes measured in the crustal fields at Mars by the MGS magnetometer/electron reflectometer instrument with a B field-dependent transport code, *Journal of Geophysical Research (Planets)*, *108*, 5134, doi:10.1029/2003JE002158.

Liemohn, M. W., et al. (2006), Mars Global MHD Predictions of Magnetic Connectivity Between the Dayside Ionosphere and the Magnetospheric Flanks, *Space Sci. Rev.*, *126*, 63–76, doi:10.1007/s11214-006-9116-8.

Liemohn, M. W., et al. (2007), *Mars Global MHD Predictions of Magnetic Connectivity between the Dayside ionosphere and the Magnetospheric Flanks*, p. 63, doi:10.1007/978-0-387-70943-7-4.

Lundin, R., et al. (2006a), Ionospheric plasma acceleration at Mars: ASPERA-3 results, *Icarus*, *182*, 308–319, doi:10.1016/j.icarus.2005.10.035.

Lundin, R., et al. (2006b), Plasma Acceleration Above Martian Magnetic Anomalies, *Science*, *311*, 980–983, doi:10.1126/science.1122071.

Lundin, R., et al. (2006c), Auroral Plasma Acceleration Above Martian Magnetic Anomalies, *Space Sci. Rev.*, *126*, 333–354, doi:10.1007/s11214-006-9086-x.

Mitchell, D. L., et al. (2016), The MAVEN Solar Wind Electron Analyzer, *Space Sci. Rev.*, *200*, 495–528, doi:10.1007/s11214-015-0232-1.

Richards, P. G., and W. K. Peterson (2008), Measured and modeled backscatter of ionospheric photoelectron fluxes, *Journal of Geophysical Research (Space Physics)*, *113*, A08321, doi:10.1029/2008JA013092.

Vignes, D., et al. (2000), The solar wind interaction with Mars: Locations and shapes of the bow shock and the magnetic pile-up boundary from the observations of the MAG/ER Experiment onboard Mars Global Surveyor, *Geophys. Res. Lett.*, *27*, 49–52, doi:10.1029/1999GL010703.

Wilson, G. R., G. Khazanov, and J. L. Horwitz (1997), Achieving zero current for polar wind outflow on open flux tubes subjected to large photoelectron fluxes, *Geophys. Res.*

Lett., *24*, 1183–1186, doi:10.1029/97GL00923.

Winningham, J. D., and C. Gurgiolo (1982), DE-2 photoelectron measurements consistent with a large scale parallel electric field over the polar cap, *Geophys. Res. Lett.*, *9*, 977–979, doi:10.1029/GL009i009p00977.

Xu, S. (2015), Superthermal electrons at Mars: Photoelectrons, solar wind electrons, and dust storm influences, Ph.D. thesis, University of Michigan.

Xu, S., and M. W. Liemohn (2015), Superthermal electron transport model for Mars, *Earth and Space Science*, *2*, 47–64, doi:10.1002/2014EA000043.

Xu, S., M. W. Liemohn, W. K. Peterson, J. Fontenla, and P. Chamberlin (2015), Comparison of different solar irradiance models for the superthermal electron transport model for Mars, *Planet. Space. Sci.*, *119*, 62–68, doi:10.1016/j.pss.2015.09.008.

Xu, S., M. Liemohn, S. Bougher, and D. Mitchell (2016), Martian high-altitude photoelectrons independent of solar zenith angle, *Journal of Geophysical Research (Space Physics)*, *121*, 3767–3780, doi:10.1002/2015JA022149.

Figure 1. Schematic of a hypothetical trans-terminator magnetic field line, with 20 V electric potential drop on the nightside, and its effect on three particles; electron №1, born with an energy of 30eV and impacting the nightside ionosphere; electron №2, born with an energy of 20 eV and being reflected back to the dayside; and an ion (i^+) born with an energy of 20 eV, and accelerated by the potential drop into the nightside ionosphere.

Figure 2. Sketches showing the predicted spectra of photo-electrons in the tail of Mars for two hypothetical electric potential drops: Panel A.) Electric potential drop $\phi < 3V$ above *MAVEN*; Panel B.) Electric potential drop $\phi = 20V$ above *MAVEN*. The predicted spectra of electrons flowing outwards from the dayside source region are shown in red, and the hypothetical spectra of electrons flowing back from the night side in blue.

Figure 3. Map of *MAVEN* orbit № 867. The co-ordinate system is Mars Solar Orbital (MSO), where x points towards the sun, y points backwards along the tangent of the planetary orbit, and z completes the right-handed set pointing up out of the plane of the ecliptic out of the northern hemisphere. The orbit of the *MAVEN* Mars Scout is shown in maroon, with a model bow shock and magnetic pileup boundary (ionopause) in black, according to *Vignes et al.* [2000].

Table 1. Preliminary survey of Trans-terminator potential drops

Orbit №	Date/Time (GMT)	Alt.(km)	SZA. (°)	Φ_{TOTAL} (V)	Φ_{SC} (V)	Φ_{Mars} (V)
795	2015-02-26 14:28:03	166	96	11.5±1.0	-1.1±0.2	12.6±1.1
795	2015-02-26 14:29:51	195	102	9.0±0.8	-0.7±0.1	9.7±0.8
798	2015-02-27 04:00:41	188	100	11.5±1.0	-1.9±0.4	13.4±1.1
798	2015-02-27 04:02:17	226	104	11.5±1.0	-3.9±0.8	15.4±1.3
799	2015-02-27 08:31:25	195	101	9.0±0.8	-1.1±0.2	10.1±0.8
799	2015-02-27 08:33:27	248	106	7.2±0.6	-1.9±0.4	9.1±0.7
800	2015-02-27 13:03:47	247	106	9.0±0.8	-1.5±0.3	10.5±0.9
805	2015-02-28 11:37:00	292	108	9.0±0.8	-1.5±0.3	10.5±0.9
818	2015-03-02 22:11:18	242	100	9.0±0.8	-1.3±0.3	10.3±0.8
821	2015-03-03 11:45:25	323	106	6.5±0.5	-1.2±0.2	7.7±0.6
	Mean:	232 km	103°	9.3±0.8 V	-1.6±0.6 V	10.9±0.9 V

Figure 4. Magnetic and electron observations from the NASA *MAVEN* Mars Scout on orbit №867. A - Spacecraft altitude; B - MAVEN Magnetometer observations in the Mars Solar Orbital coordinate system; Panel C - Electron spectrogram from MAVEN SWEA; and three electron scans (α, β, γ), showing energy vs. differential energy flux and energy vs. the ratio between outflowing and inflowing electron fluxes. Scan α - Closed magnetic field line with both footpoints in the dayside ionosphere; Scan β - Closed trans-terminator magnetic field line with no evidence of an electric potential drop; Scan γ - Closed trans-terminator magnetic field line with a 7V electric potential drop.

Figure 5. Full pitch-angle distributions for each of the three electron scans: Scan α - Closed magnetic field line with dayside photoelectron sources at both ionospheric footpoints; Scan β - Closed trans-terminator magnetic field line with a single source of photoelectrons on the dayside, and backscattered photoelectrons returning from the nightside resulting in an anisotropic distribution; Scan γ - Closed trans-terminator magnetic field line with a single source on the dayside ionosphere, and semi-isotropy below 7eV resulting from electrostatic mirroring.

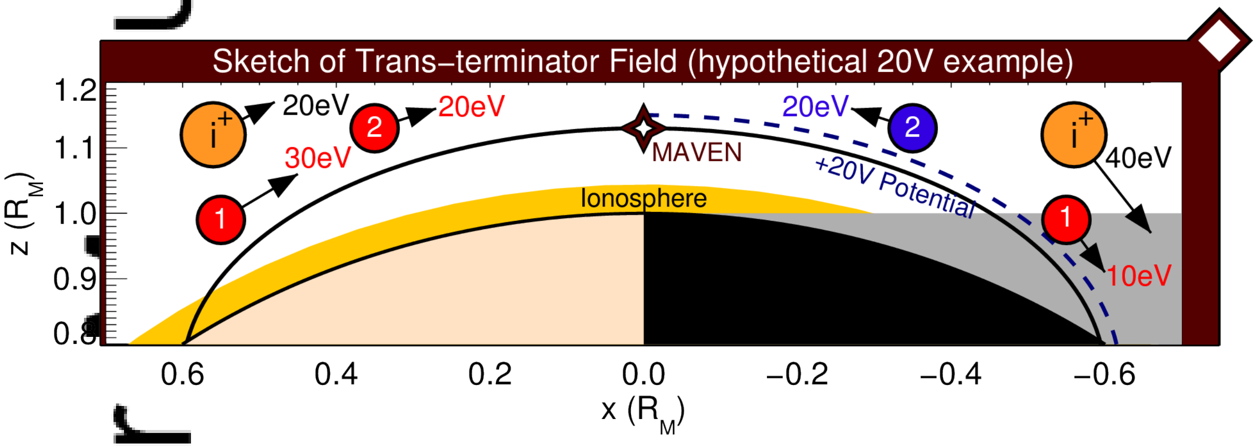

2016ja023589-f01-z-.eps

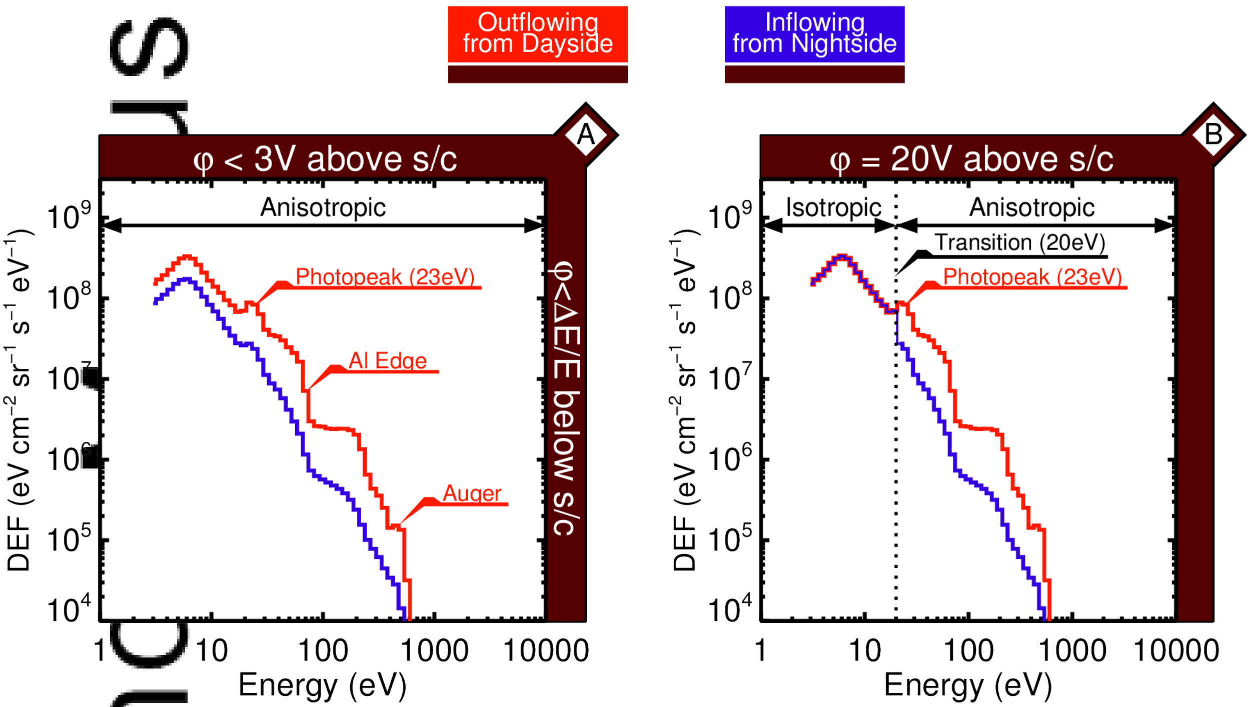

2016ja023589-f02-z-.eps

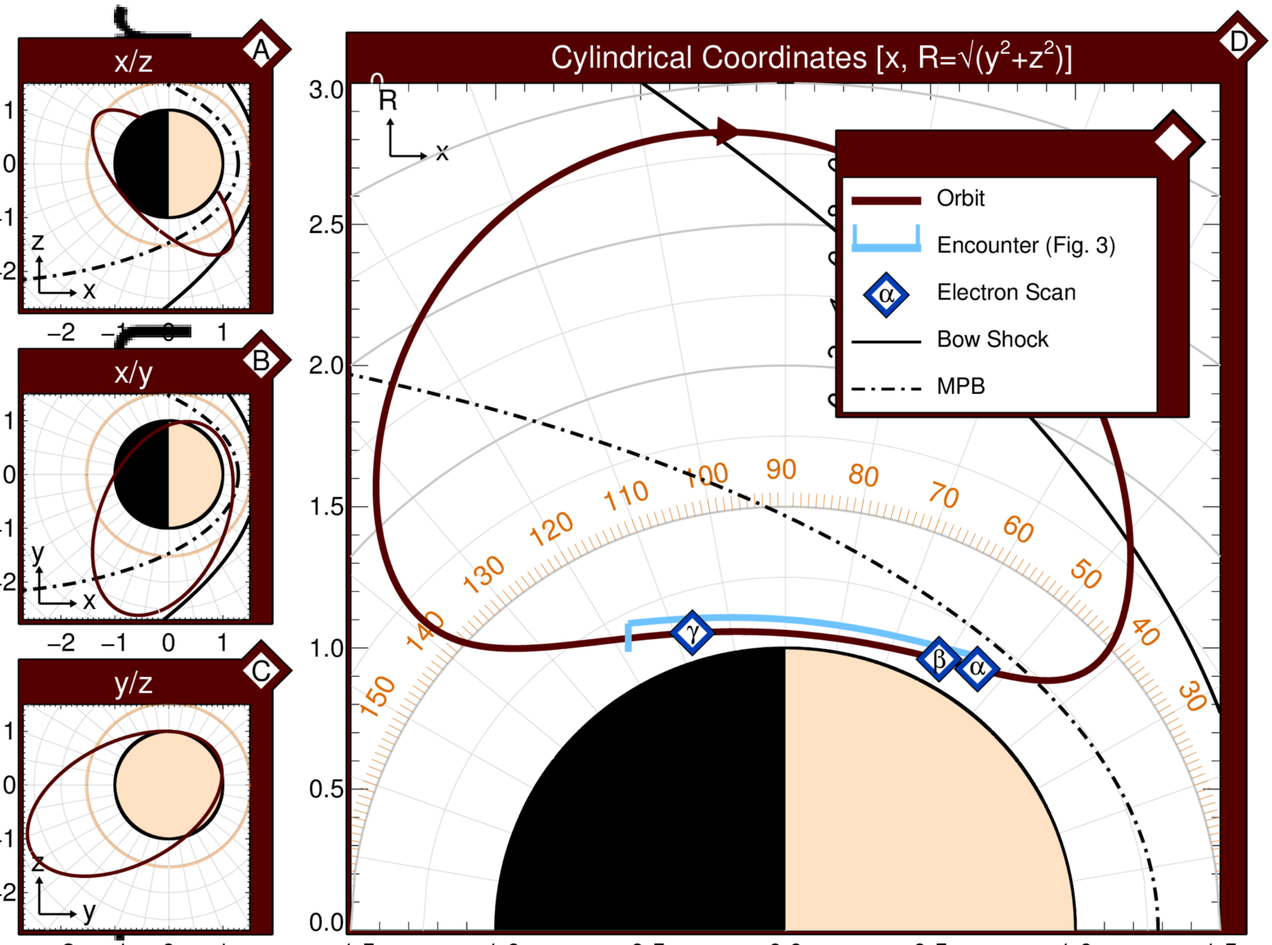

2016ja023589-f03-z-.eps

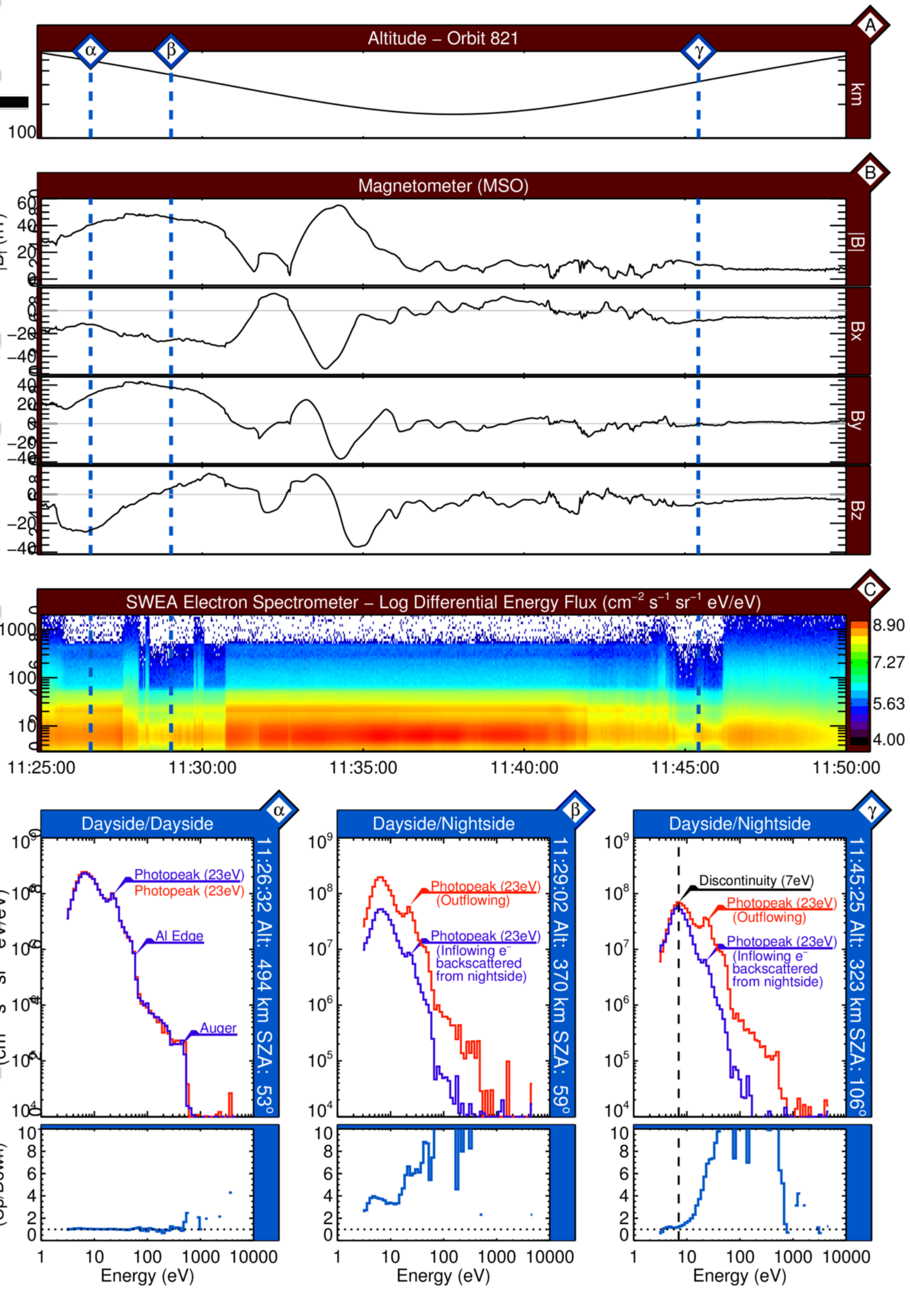

2016ja023589-f04-z-.eps

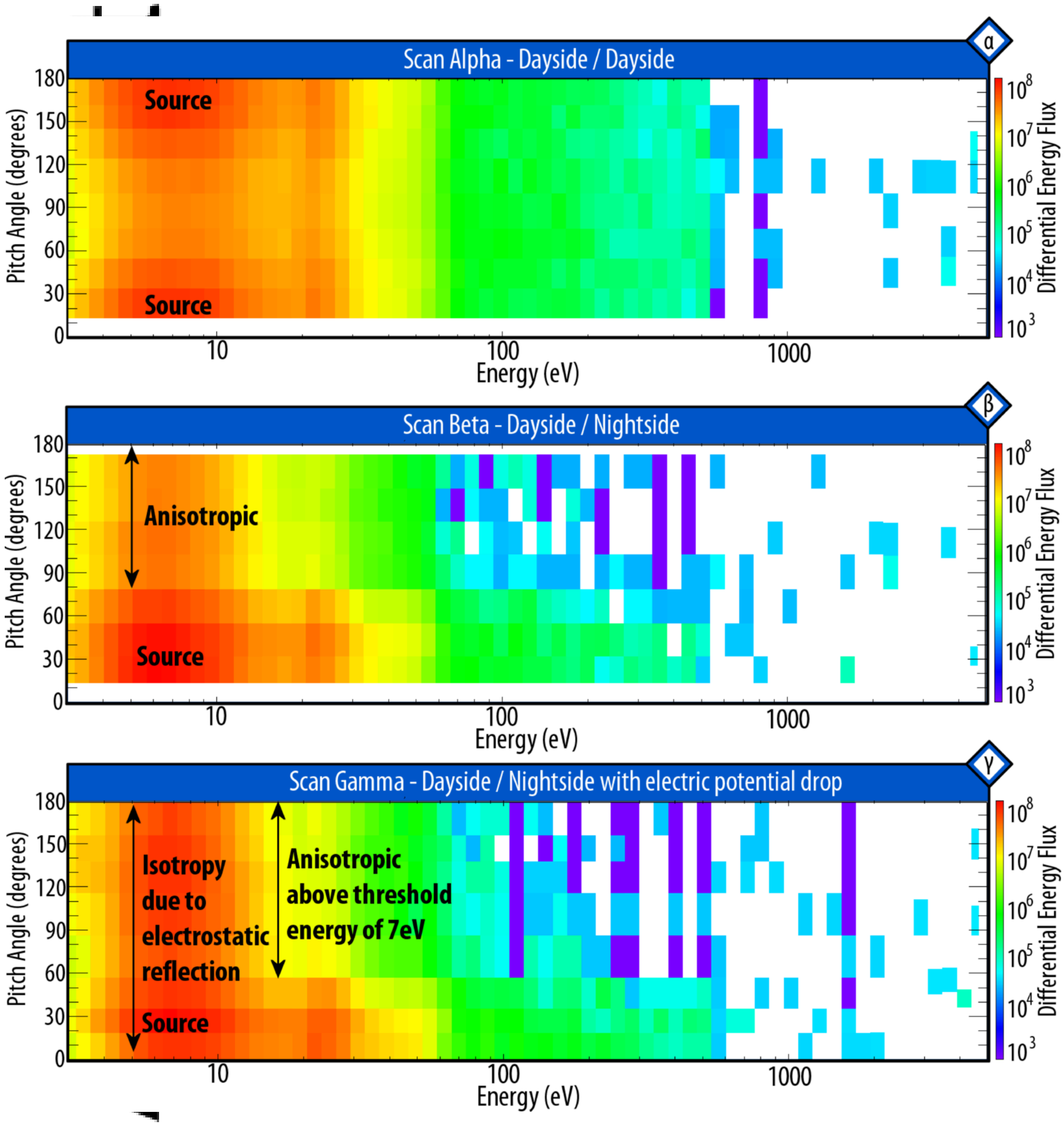

2016ja023589-f05-z-.eps